Inverted Method for Simulation of Electrokinetic Transport in Microchannel Devices

Robert H. Nilson and Stewart K. Griffiths
Sandia National Laboratories
rhnilso@sandia.gov and skgriff@sandia.gov
Livermore, CA 94551-0969

ABSTRACT

An inverted method of solution is used to numerically solve the equations governing electrokinetic fluid flow and species transport in microscale turns, junctions and curved channels. Rather than solving for the electric potential and fluid velocity on the physical x-y plane, the spatial coordinates are treated as the dependent variables on the plane of the electric potential, ϕ, and the associated stream function, ψ. Transport and dispersion of analyte samples are computed by tracking tracer particles that move by both advection and diffusion. The advantage of this inverted approach is that curved or complex channel boundaries become straight lines on the $\phi-\psi$ domain. This facilitates rapid solution of the governing equations and permits variation of the channel geometry without regridding. The method is used to optimize the shapes of low-dispersion turns. These reduce sample dispersion by two to three orders of magnitude relative to conventional geometries.

Keywords: microfluidics, simulation, transport, flow, turns inverted, design, optimized, dispersion, electroosmosis

1 INTRODUCTION

Microchannel devices are currently under development for detection, analysis, and synthesis of chemical and biological species. In these devices, electrokinetic fluid motion and species transport cause only minimal dispersion of sample bands moving along straight channel sections. This is because the velocity profile is nearly uniform across the channel when the Debye layers are thin compared to the channel width. In passing through turns and junctions, however, sample bands suffer severe distortion and elongation resulting from variations in path length and fluid speed across the channel.

Although such dispersion degrades system performance, it can be minimized by the use of tailored turns, junctions, and transitions that have been optimized through iterative design simulations. To this end we have developed an inverted approach to solving the equations governing fluid flow and species transport in channels of arbitrary shape. The computational problem is posed on the rectangular domain of the electric potential and the complementary stream function thereby facilitating the iterative evolution of the channel boundaries to an optimized low-dispersion geometry.

The methodology presented here has been verified by comparison with analytical solutions and with experimental results from others for band spreading in conventional turns [1]. The method has also been used to design optimized turns that reduce dispersion by two to three orders of magnitude [2]. The focus of the present paper is on methodology; here we provide the mathematical detail necessary for successful implementation, as well as several results.

2 GOVERNING EQUATIONS

For an incompressible fluid with constant properties, the transport of an inert chemical species is governed by

$$\frac{\partial c}{\partial t} + \mathbf{u}\cdot\nabla c = D\nabla^2 c \qquad (1)$$

where c is the species concentration, t is time, $\mathbf{u} = u\mathbf{i} + v\mathbf{j}$ is the local fluid velocity, and D is the diffusivity. In most microfluidic devices, the flow is driven by electrokinetic rather than pressure forces, Reynolds numbers are very small, and the flow field is usually quasi-steady. Under these conditions, the momentum equation and the Poisson equation governing the electric potential, ϕ, are

$$\mu\nabla^2\mathbf{u} = \rho_e\nabla\phi \qquad \text{and} \qquad \varepsilon\nabla^2\phi = -\rho_e \qquad (2)$$

where μ is the fluid viscosity, ρ_e is the charge density and ε is the dielectric constant.

In many cases of practical interest, the local fluid velocity in electroosmotic flow is proportional to the applied electric field [3]. The main conditions necessary for such similitude are: (1) a quasi-steady electric field; (2) a Debye layer that is thin compared to any channel dimension; (3) uniform fluid properties in the neutral fluid outside the Debye layer; and (4) solid bounding surfaces that are electrically non-conducting and have a uniform surface charge or surface potential. Under these conditions, commonly satisfied, the electric potential outside the Debye layer is governed by the Laplace equation and the velocity is proportional to the electric field.

$$\nabla^2\phi = 0 \qquad \text{and} \qquad \mathbf{u} = -\frac{\varepsilon\zeta}{\mu}\nabla\phi \qquad (2)$$

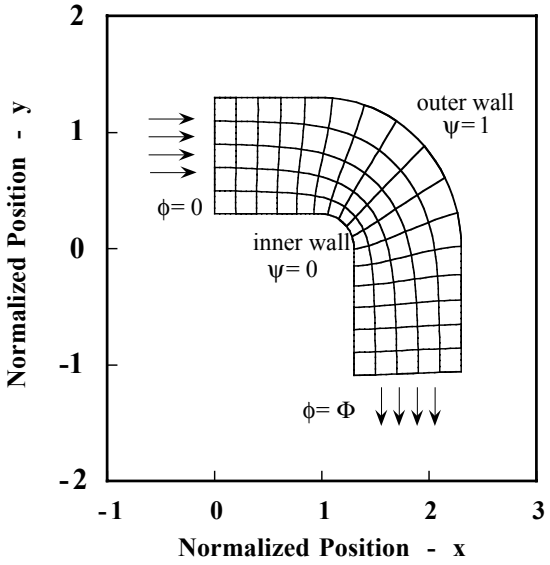

Figure 1. Streamlines and isopotential lines plotted on physical x-y plane. Turns and junctions are needed for interconnections and to fold long channels onto small chips

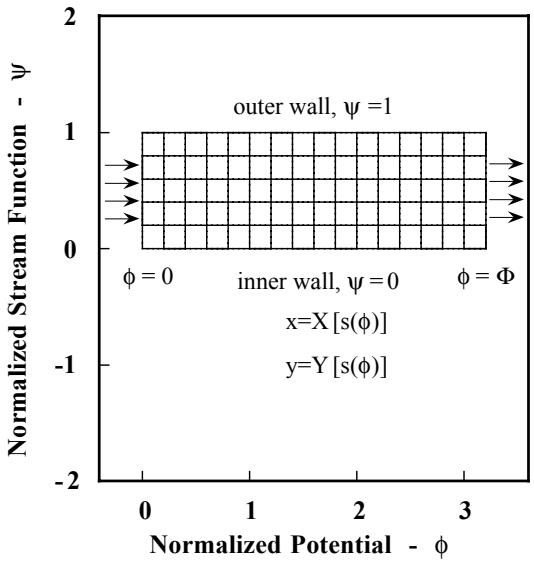

Figure 2. Streamlines and isopotential lines plotted on computational ϕ–ψ domain. Rectangular domain simplifies calculations and iterative optimization of geometry.

Here, ζ is the potential difference across the Debye layer. Thus, it is only necessary to solve the Laplace equation and to use the computed electric field to deduce the corresponding velocity field. Moreover, when the above restrictions are satisfied, the electric potential and fluid velocity in any two-dimensional channel bounded by parallel planes is strictly two-dimensional and is independent of the channel depth [3]. Most flows in microfluidic channels satisfy all of the above conditions, at least on the scale of the turns and junctions of interest here.

The preceding equations were developed in the context of neutral species transport in electroosmotic flow. However, because the electroosmotic fluid velocity is proportional to the electric field, these governing equations are essentially the same as those describing electrophoretic motion of a single charged species relative to a stationary phase. They are also applicable to cases where the velocity field is proportional to the pressure gradient, as in porous materials and in high aspect ratio channels.

3 NUMERICAL APPROACH

To simplify the analysis of analyte transport in curved channels and turns we have developed a novel inverted method of solution. Rather than solving for the electric potential and fluid velocity on the physical x-y plane, the spatial coordinates are treated as the dependent variables on the plane of the normalized electric potential, ϕ, and the associated stream function, ψ. The advantage of this inverted approach is that curved or complex channel boundaries, like those shown in Figure 1, become straight lines on the ϕ–ψ domain, as illustrated in Figure 2. This eliminates the need for adaptive gridding, improves the accuracy of the numerical discretization, and permits iterative adjustment of channel geometry to reduce sample dispersion.

Since ϕ and ψ satisfy the Laplace equation on the x-y domain, it follows from the properties of harmonic functions that x and y satisfy the Laplace equation on the ϕ–ψ domain.

$$\frac{\partial^2 x}{\partial \phi^2} + \frac{\partial^2 x}{\partial \psi^2} = 0 \qquad \text{and} \qquad \frac{\partial^2 y}{\partial \phi^2} + \frac{\partial^2 y}{\partial \psi^2} = 0 \tag{3}$$

In addition to these governing equations, the functions x(ϕ,ψ) and y(ϕ,ψ) must also satisfy the following Cauchy-Riemann compatibility relations,

$$\frac{\partial x}{\partial \phi} = \frac{\partial y}{\partial \psi} \qquad \text{and} \qquad \frac{\partial x}{\partial \psi} = -\frac{\partial y}{\partial \phi} \tag{4}$$

These are used in mapping boundary conditions between the physical and inverted domains.

The geometry of the inner and outer channel walls is defined in a fully general manner by prescribing the x and y coordinates in terms of the arc length, s, along each surface.

$$x = X(s) \qquad \text{and} \qquad y = Y(s) \tag{5}$$

In the numerical implementation the shape functions, X(s) and Y(s), describing each surface are generated in a discrete form by processing a list of x and y coordinates representing points on the surface, computing the distance between points, and adding these increments to obtain the cumulative arc length associated with each (X,Y) pair. A pair of lists defining the inner and outer surfaces are generated prior to the solution. However, to apply these

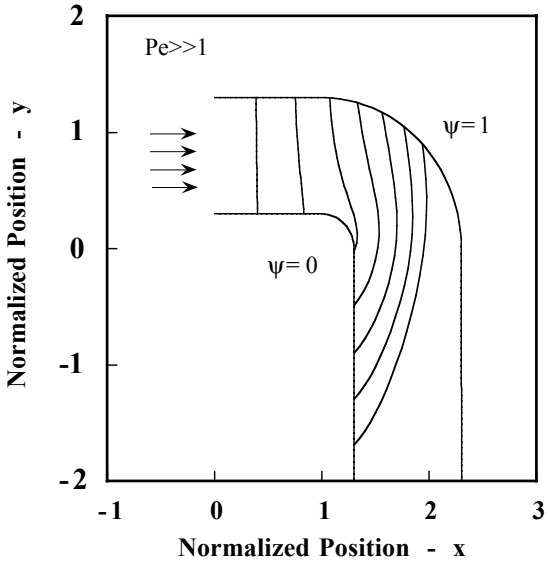

Figure 3. Computed distortion of a narrow sample band traversing a turn. At high Peclet numbers, tracer particles move along streamlines at the local electrokinetic speed.

conditions on the $\phi-\psi$ domain requires knowledge of the function $s(\phi)$ describing the variation of arc length with potential along each of the channel walls. This function is determined as a part of the overall solution procedure.

The governing Laplace equations (3) for x and y are discretized on a uniform square mesh that covers the rectangular problem domain. Since convergence is very rapid, single-point Gauss-Sidel iteration is quite adequate. Similarly, although accuracy can be improved by using higher-order finite-difference representations of the Laplace operator, each interior point can be updated by simply taking the average of the four nearest neighbors. The convergence rate is determined mainly by the evolution of the boundary conditions on the channel walls.

To ensure convergence of the boundary conditions, the two complementary field problems for $x(\phi_i,\psi_j)$ and $y(\phi_i,\psi_j)$ are solved in an alternating fashion. Beginning from an initial guess of the arc lengths, $s_i(\phi_i)$, for the boundary points on each of the channel walls, we interpolate the lists, $X_k(s_k)$, to obtain the corresponding boundary values, $x_i(\phi_i)$. These boundary conditions are used to compute the corresponding field, $x(\phi_i,\psi_j)$. The arc lengths, $s_i(\phi_i)$, along the channel walls are then recomputed using the cartesian increments

$$\Delta x_i = x_i - x_{i-1} \qquad \text{and} \qquad \Delta y_i = -\left.\frac{\partial x}{\partial \psi}\right|_{i-1/2} \Delta\phi_i \qquad (7)$$

The latter of these is based on the Cauchy-Reimann condition (4b) and makes use of the numerically calculated surface normal derivative. The boundary lists, $Y_k(s_k)$, are next interpolated at the newly estimated arc length values, $s_i(\phi_i)$, and the resulting $y_i(\phi_i)$ are used as boundary values in solving for $y(\phi_i,\psi_j)$. In the final step, the arc length is recomputed using Δy increments from the current solution together with Δx increments computed from the Cauchy-Riemann condition, (4a), and surface normal derivative of $y(\phi_i,\psi_j)$. The entire procedure is then repeated to convergence. Boundary conditions on the inflow and outflow boundaries may generally be set by assuming a linear variation of x or y with ψ between the values that are set on the ends of the solid channel boundaries. Execution time for a typical turn with a mesh having 41 points across the channel is typically a few seconds.

4 EXAMPLE CALCULATIONS

The streamlines and isopotentials shown in Figure 1 were plotted by simply joining all of the computed points (x_{ij},y_{ij}) having a fixed i or j. Every fourth line is included in Figure 1. Dispersion of sample bands passing through a turn is computed by tracking tracer particles carried by the flow. The simplest version of this, illustrated in Figure 3, is applicable for large values of the Peclet number, Pe=Uw/D, based on the nominal speed of electrokinetic transport, U, the channel width, w, and the diffusivity, D. This parameter represents the ratio of electroosmotic or electrophoretic transport to that by diffusion.

In the high Peclet number example of Figure 3, single tracer particles are released simultaneously on each of the streamlines. Each tracer is translated along the streamline at the local transport speed computed from equation (2b) using the local potential gradient. This process is simplified by the present inverted approach because the required derivatives of the potential and the direction of particle translation are always along the grid lines. At specified times, the tracers are joined by lines to show the sample profile. As seen in Figure 3 the sample band leaving the turn is severely elongated, making it difficult to distinguish the arrival times of different sample species traveling at slightly different speeds, thereby reducing the resolution of electrophoretic or electrochromatographic separation devices.

As illustrated in Figure 4, the influence of diffusion may be described by releasing a large number of tracer particles which are incrementally advanced both by electrokinetic transport along local streamlines and by diffusion steps having components in both the ϕ and ψ directions. This Monte Carlo method is advantageous in the study of band spreading because it does not introduce the artificial numerical dispersion generated by traditional finite difference and finite element approaches. Each translation of a tracer particle includes an advective contribution of length $Su\Delta t$ based on the local speed, u, and time step, Δt, as well as a pair of orthogonal diffusion steps having lengths $RSD(\Delta t/2)^{1/2}$ where R is a normally-distributed random variable having a mean of zero and variance of one; S is the local scale factor relating spatial steps to steps in $\Delta\phi$ and $\Delta\psi$. All of these steps take place in the orthogonal ϕ and ψ coordinate system.

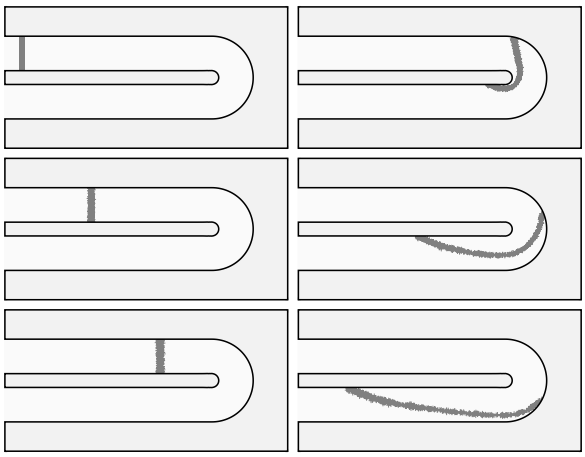

Figure 4. Band spreading at high Peclet number results from differences in path length and speed of transport along inner and outer walls. Skewing of sample profile results in a total turn-induced normalized variance of $(\sigma/w)^2 \sim 3.9$.

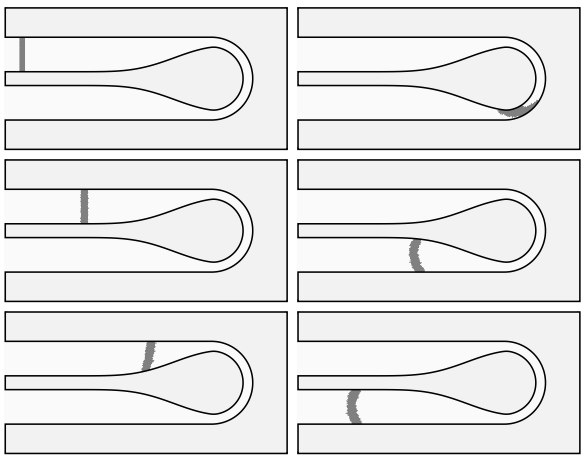

Figure 5. Low-dispersion turn dramatically reduces sample skewing. One-sided tapers of contraction and expansion regions produce reverse skewing offsetting that induced by the turn, reducing variance to $(\sigma/w)^2 \sim 0.0025$.

The results shown in Figure 4 illustrate sample dispersion in a 180° turn for a Peclet number of 10000. The series of frames, read from top to bottom along both columns, are spaced equally in time. As in Figure 3, the portion of the sample traveling along the inner radius completes the turn first, followed progressively by portions closer to the outer channel wall. In contrast to Figure 3, we see that longitudinal diffusion has already spread the band somewhat before it reaches the turn and that transverse diffusion is beginning to spread the elongated band across the channel downstream of the turn. These affects of diffusion would be much greater at the smaller Peclet numbers commonly used in microfluidic devices. A large Peclet number was chosen here to better illustrate the benefit of an optimized channel geometry.

5 LOW-DISPERSION TURNS

The turn-induced sample dispersion illustrated in Figure 4 can be substantially reduced by reshaping the channel walls. In performing this optimization, the boundary locations are represented parametrically by analytical expressions. In the example of Figure 5, the inner wall of the turn is represented by a four-parameter profile. The parameters are the minimum channel width, the length of the expansion and contraction regions, the angular extent of a turning region having a constant radius of curvature, and a shape parameter that controls the contour of the expansion and contraction regions. The outer wall is held fixed.

Spreading of the species distribution is computed from the final position of the tracer particles once all have traversed the turn. The normalized variance, $(\sigma/w)^2$, is determined by first computing the mean axial position and then summing the squares of deviations from the mean. The variance is minimized by use of a nonlinear minimization algorithm that iteratively adjusts the profile parameters. The speed of the present inverted approach is essential to the method because a full minimization often entails hundreds of simulations for different geometries. However, a well-optimized turn can reduce dispersion by two to three orders of magnitude as seen by comparing Figure 4 and 5.

6 SUMMARY

A novel inverted method of solution has been used to solve the equations governing electrokinetic flow and species transport in microfluidic turns. The problem is posed on the rectangular domain of the electric potential and the complementary stream function thereby facilitating the iterative evolution of the boundary shape toward an optimum geometry that minimizes sample dispersion. Sample transport is computed using tracer particles that move by advection and diffusion. The method is used to design low-dispersion turns that reduce sample band dispersion by two to three orders of magnitude relative to conventional turns.

ACKNOWLEDGMENT

This work was funded by a Sandia Phenomenological Modeling and Engineering Simulations LDRD. Sandia National Laboratories is operated by Sandia Corporation for the US DOE under contract DE-AC04-94AL85000.

REFERENCES

[1] S. K. Griffiths and R. H. Nilson, *Anal. Chem. 72,* 5473-5482, 2000.

[2] S. K. Griffiths and R. H. Nilson, *Anal. Chem.*, Web ASAP Article, Dec. 8, 2000.

[3] E. B. Cummings, S. K. Griffiths, R. H. Nilson, and P. H. Paul, *Anal. Chem. 72*, 2526-2532, 2000.